

# MgII radius-luminosity relation: applications to the BLR structure and cosmology

Michal Zajaček

**B. Czerny, N. Khadka, M. L. Martínez-Aldama, S. Panda, R. Prince, B. Ratra,  
M. Naddaf**

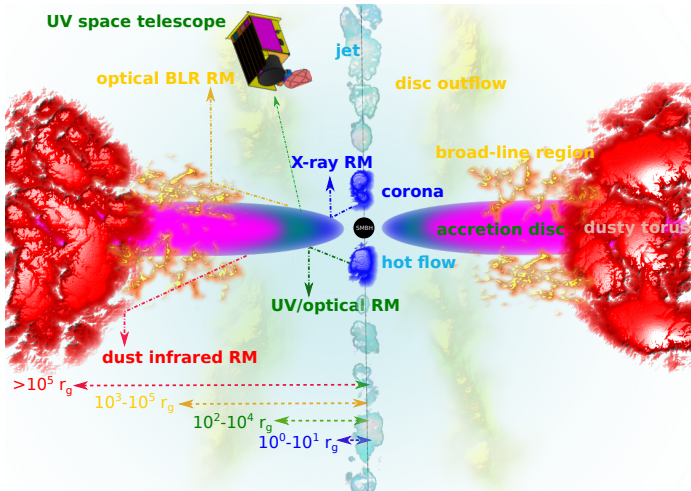
Faculty of Science, Masaryk University

The Restless Nature of AGN ✦ 10 years later

June 27, 2023 - Napoli

# Reverberation mapping of galactic nuclei

Different wavelengths probe different scales of an accretion flow



# Reverberation mapping of galactic nuclei – results

- **mean radius of the BLR:**  $R_{\text{BLR}} \sim c\tau_{\text{rest}}$
- **the virial mass of the SMBH:**  $M_{\text{vir}} = \frac{f_{\text{vir}}c\tau_{\text{rest}}\text{FWHM}^2}{G}$
- **radius-luminosity relation:**  $R_{\text{BLR}} = CL_{\text{mon}}^\gamma \rightarrow \tau = \beta + \gamma \log L_{\text{mon}}$

The power-law slope is expected to be close to 0.5.

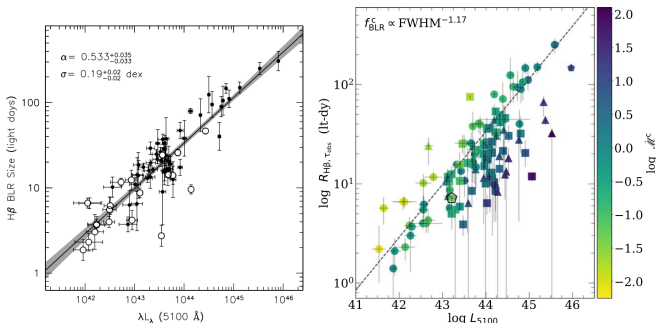
This follows from simple photoionization theory of a BLR cloud:

$$U = \frac{Q_{\text{ion}}(H)}{4\pi R^2 c n_e}, \quad Q_{\text{ion}}(H) = \int_{\nu_i}^{+\infty} \frac{L_\nu}{h\nu} d\nu$$

Under the assumption  $Un_e \sim \text{konst.}$  for different sources, we can derive  $R \propto L^{1/2}$

# H $\beta$ Radius-luminosity relation

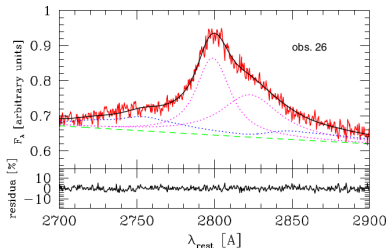
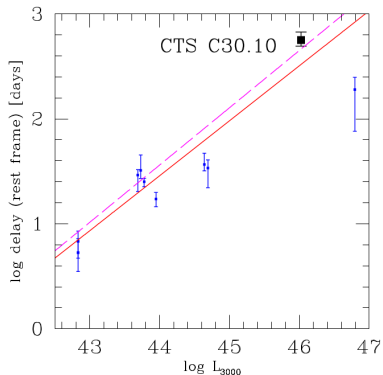
- H $\beta$  broad line was mostly used to obtain time delays for lower-redshift sources ( $0.0023 \leq z \leq 0.89$ ).
- Earlier data had a small scatter (lower accreting, variable sources), later the scatter increased due to the presence of higher-accreting sources.



Bentz+13 (71 sources) and Martinez-Aldama+2019 (117 sources)

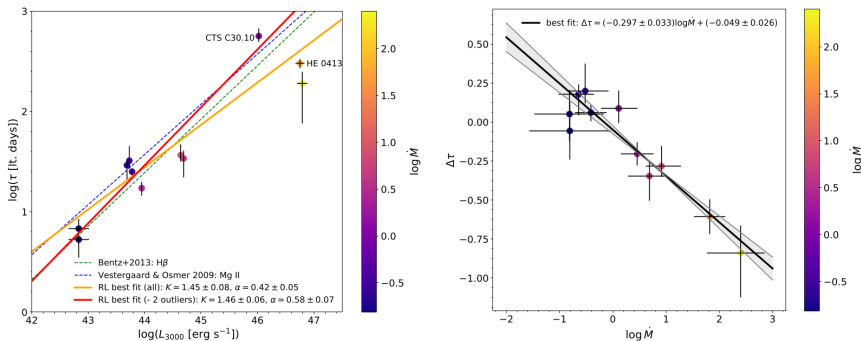
# MgII Radius-luminosity relation

- Czerny+2019, Zajaček+2020, and Zajaček+2021 construct first robust MgII radius-luminosity relations using higher-redshift, luminous sources in the range  $0.0033 \leq z \leq 1.89$ .
- 10 sources (2xNGC 4151, 6 SDSS-RM, CT252 and CTS C30.10:  $\tau = 562^{+116}_{-68}$  days)



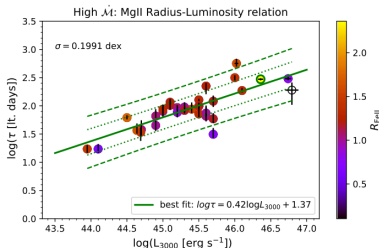
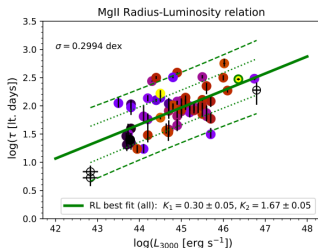
# MgII Radius-luminosity relation

- Zajaček+2020 add one more measurement (HE 0413,  $z = 1.37648$ ,  $\tau = 302.6_{-33.1}^{+28.7}$  days) and show that the departure is correlated with the accretion rate
- Correlation:  $\dot{M} = 26.2(L_{44}/\cos\theta)^{3/2}m_7^{-2}$ ,  $\Delta\tau = \log(\tau_{\text{Obs}}/\tau_{\text{RL}})$



# MgII Radius-luminosity relation

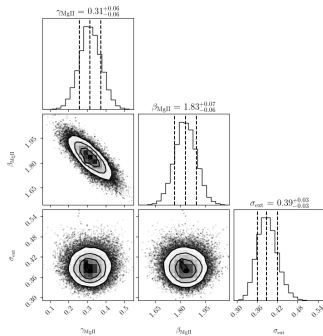
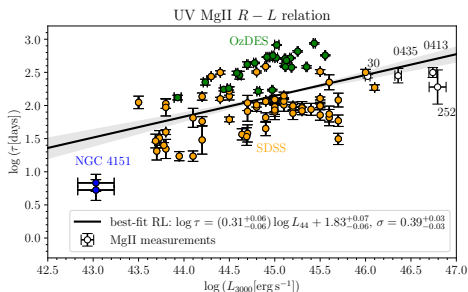
- In Zajaček+2021, we perform reverberation mapping of the quasar HE 0435 ( $z = 1.2231$ ,  $\tau = 296_{-14}^{+13}$  days)
- 57+6 SDSS-RM (Homayouni+20, Shen+16), 2xNGC4151 (Metzroth+06), CT 252 (Lira+18), CTS C30.10, HE 0414, HE 0435: 69 sources



$\log \tau_{\text{obs}}$	$K_1$	$K_2$	$K_3$	$\sigma_{\text{rms}}$ [dex]	$r$	$\sigma_{\text{rms}}$ [dex] (without)	$r$ (without)
$K_1 \log L_{44} + K_2$	$0.422 \pm 0.055$	$1.374 \pm 0.082$	...	0.1991	0.80	0.2012	0.78
$K_1 \log L_{44} + K_2 \log \text{FWHM}_3 + K_3$	$0.43 \pm 0.06$	$-0.13 \pm 0.31$	$1.44 \pm 0.17$	0.1986	0.80	0.2007	0.78
$K_1 \log L_{44} + K_2 \log R_{\text{Fe II}} + K_3$	$0.45 \pm 0.05$	$0.84 \pm 0.29$	$1.28 \pm 0.08$	0.1734	0.85	0.1718	0.84
$K_1 \log L_{44} + K_2 \log R_{\text{H}\alpha} + K_3$	$0.39 \pm 0.06$	$-0.38 \pm 0.18$	$0.99 \pm 0.19$	0.1861	0.83	0.1863	0.82

# MgII Radius-luminosity relation

Combining 69 sources with 25 OzDES measurements (Yu+23), we obtain 94 measurements with the redshift range of  $0.0041 \leq z \leq 1.89$  (see Prince+2023)

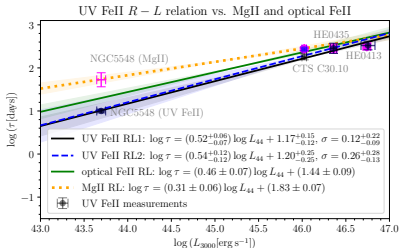
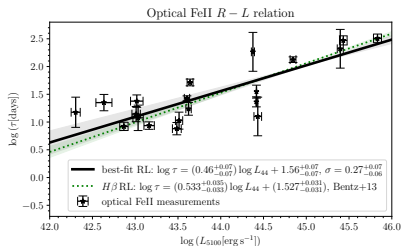


MgII R-L relation and the 2D and 1D likelihood distributions



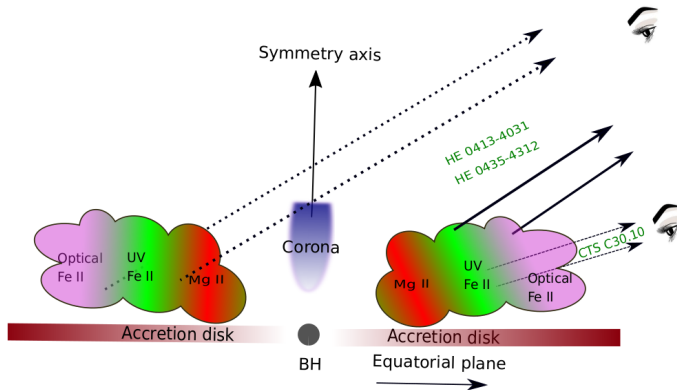
# Comparison of MgII and FeII R-L relations

- first UV FeII R-L relation based on 4 measurements presented in **Prince+(2023)**
- comparison with optical FeII and MgII R-L relations
- NGC 5548: UV FeII time delay by Maoz+1993, MgII by Clavel+1991



## Optical and UV FeII R-L relations vs. MgII R-L relation

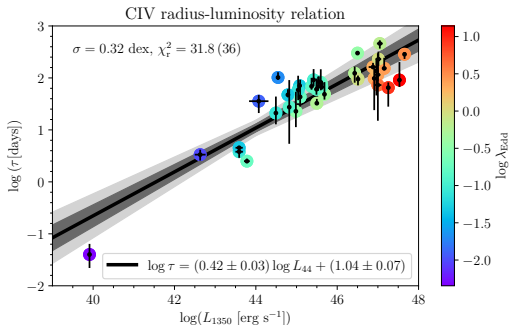
# Comparison of MgII and FeII R-L relations: distribution



R-L relations + wavelength-resolved RM (Prince+22,23)

# CIV Radius-luminosity relation

First constrained HIL radius-luminosity relation,  $0.001064 \leq z \leq 3.368$ , 38 sources were collected and analyzed by Kaspi et al. (2021).



Taken from Cao, Zajaček et al. (2022)

# Datasets

## RM QSO data

applied for **simultaneously constraining R-L relation as well as cosmological model parameters**. A better established BAO+ $H(z)$  combined sample was used as a comparison sample.

Sample	Source number	Redshift range	Reference
$H\beta$ RM QSOs	118	$0.0023 \leq z \leq 0.89$	Khadka+22
MgII RM QSOs	69/78	$0.0033 \leq z \leq 1.89$	Khadka+21
CIV RM QSOs	38	$0.001064 \leq z \leq 3.368$	Cao+22
BAO	12	$0.122 \leq z \leq 2.334$	Cao & Ratra 2022
$H(z)$	32	$0.07 \leq z \leq 1.965$	

**Table:** Overview of used RM QSO data and the BAO+ $H(z)$  comparison sample. BAO+ $H(z)$  data are adopted from Tables 1 and 2 in Cao & Ratra 2022, MNRAS, vol. 513, p. 5686-5700.

## RM QSOs as standardizable candels

1. Perform reverberation mapping  $\rightarrow$  continuum–broad line time lag  $\tau_{\text{obs}}$
2. Use radius–luminosity (R-L) relation to calculate theoretical time lags  $\tau_{\text{th}}$

$$\log \left( \frac{\tau_{\text{th}}}{\text{day}} \right) = \beta + \gamma \log \left[ \frac{L_{\text{mon}}(z, \mathbf{p})}{10^{44} \text{ erg s}^{-1}} \right],$$

$L_{\text{mon}} = 4\pi D_L(z, \mathbf{p})^2 \lambda F_\lambda$ , where the luminosity distance is a function of the cosmological expansion rate  $H(z, \mathbf{p})$ , which depends on the considered cosmological model.

3. Maximize likelihood function to find simultaneously **R-L relation**  $(\beta, \gamma)$  and **cosmological model parameters**  $\mathbf{p}$

# RM QSOs as standardizable candels

## 3. Maximize likelihood function

$$\ln LF = -\frac{1}{2} \sum_{i=1}^N \left\{ \frac{[\log \tau_i^{\text{obs}} - \log \tau_i^{\text{th}}]^2}{s_i^2} + \ln(2\pi s_i^2) \right\}$$
$$s_i^2 = \sigma_{\log \tau_{\text{obs},i}}^2 + \gamma^2 \sigma_{\log F_{3000,i}}^2 + \sigma_{\text{int}}^2$$

- 6 cosmological models: flat and non-flat  $\Lambda$ CDM, XCDM, and  $\phi$ CDM

$$H(z) = H_0 \sqrt{\Omega_{m0}(1+z)^3 + \Omega_{k0}(1+z)^2 + \Omega_{\text{DE}}(z)},$$

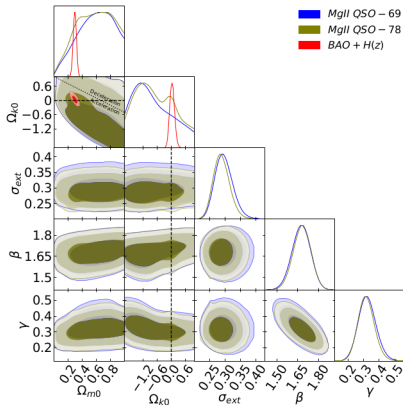
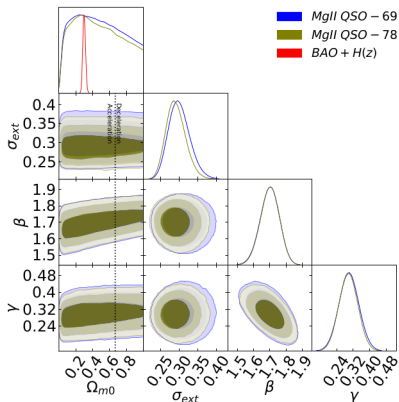
$$\text{For } \Lambda\text{CDM and XCDM: } \Omega_{\text{DE}}(z) = \Omega_{\text{DE}0}(1+z)^{1+\omega_x}$$

$\phi$ CDM (Peebles & Ratra 1988, Ratra & Peebles 1988):

$V(\phi) = \frac{1}{2} \kappa m_p^2 \phi^{-\alpha}$  represents scalar field potential energy density

$$\Omega_{\text{DE}} = \Omega_{\phi}(z, \alpha) = \frac{8\pi\rho_{\phi}}{32m_p^2 H_0^2}$$

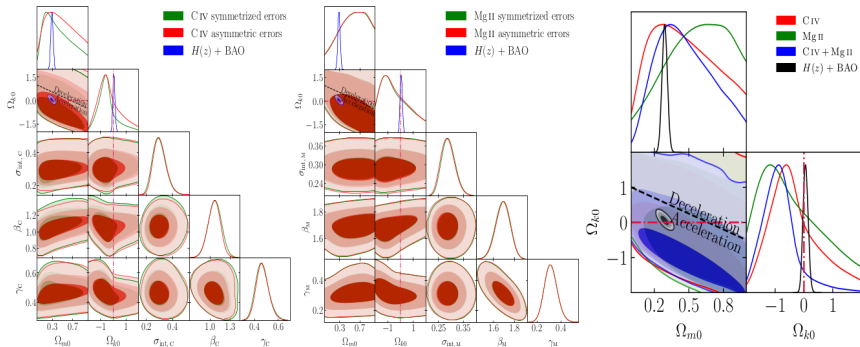
# Constraints from MglI sample



Likelihood distributions and contours for **flat (left)** and **non-flat (right)**  $\Lambda$ CDM model (see Khadka, Yu, Zajaček et al. 2021).

# Constraints from MgII+CIV+BAO+H(z) sample

Consistent with BAO+H(z) – exemplary likelihood distributions for non-flat  $\Lambda$ CDM



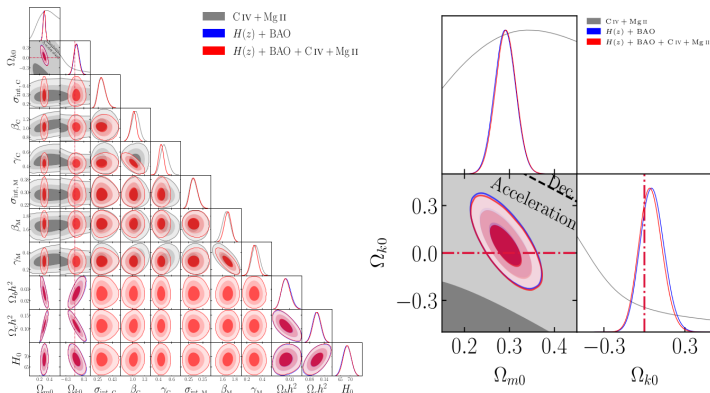
CIV and MgII quasars and their combination (Cao, Zajaček et al. 2022)



# Constraints from MgII+CIV+BAO+H(z) sample

Consistent with BAO+H(z) – exemplary likelihood distributions for non-flat  $\Lambda$ CDM

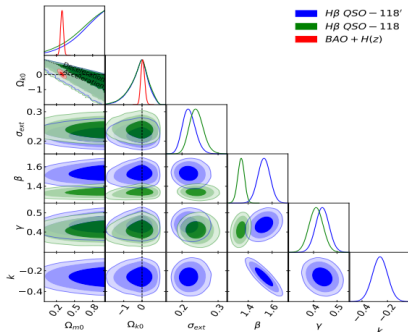
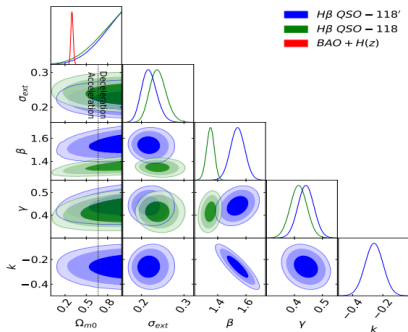
$\Lambda$ CDM



CIV and MgII quasars analyzed jointly with BAO+H(z) (Cao, Zajaček et al. 2022) → **quasars slightly tighten the constraints** ( $\sim 0.1\sigma$  at most)

# $H\beta$ sample

- lower-redshift sample
- constraints in  $\sim 2\sigma$  tension with  $\text{BAO}+H(z)$  (preference for decelerated expansion)



Likelihood contours for **flat (left)** and **non-flat (right)**  $\Lambda$ CDM model (see Khadka, Martinez-Aldama, Zajaček et al. 2022).

## Putting it all together

- Hubble diagram combining  $H\beta$ , MgII, and CIV RM QSOs with the maximum-likelihood flat  $\Lambda$ CDM model.

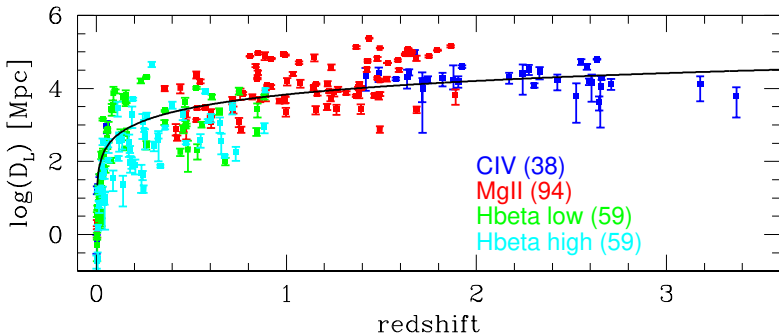


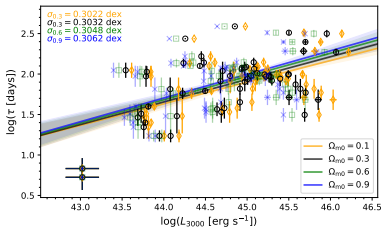
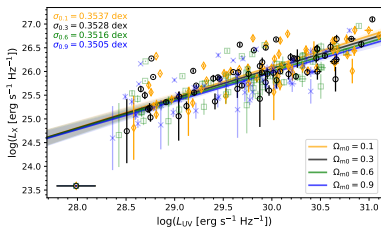
**Figure:** Hubble diagram of RM quasars ( $H\beta$ , MgII, and CIV) with the black solid line showing the inferred flat  $\Lambda$ CDM model with  $H_0 = 68.86 \text{ km s}^{-1} \text{ Mpc}^{-1}$  and  $\Omega_{m0} = 0.295$ .

## Conclusions

- MgII line is significantly variable and responds to the UV continuum emission,
- **MgII R-L relation shows a significant correlation but is flatter than both  $H\beta$  and UV FeII relations,**
- MgII (and CIV) R-L relation is independent of a cosmology model, and thus **can be applied to standardize RM quasars,**
- cosmological constraints from reverberation-mapped quasars are weaker in comparison with BAO+ $H(z)$  data,
- for MgII and CIV quasars, constraints are consistent with BAO+ $H(z)$  (Khadka et al. 2021, Cao et al. 2022). However, for  $H\beta$  quasars, there is  $\sim 2\sigma$  tension with BAO+ $H(z)$  constraints (Khadka et al. 2022),
- the joint analysis MgII+CIV+BAO+ $H(z)$  leads to mildly tighter cosmological constraints (at most  $\sim 0.1\sigma$ ) in comparison with BAO+ $H(z)$  sample alone (Cao et al. 2022).

## $R - L$ vs. $L_X - L_{UV}$ relation

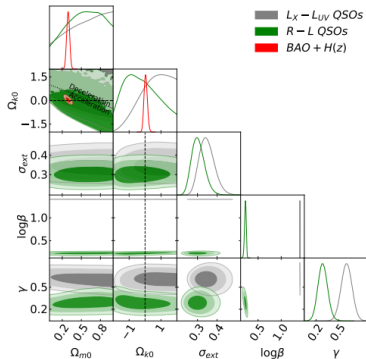
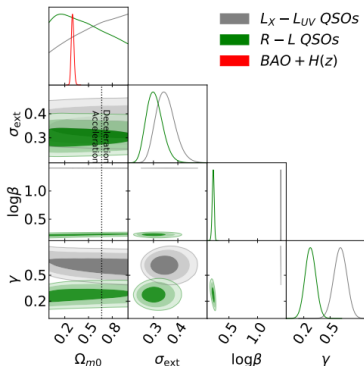
- a sample of 58 X-ray detected reverberation-mapped quasars
- systematic differences between the two relations
- $L_X - L_{UV}$  shows preference for high  $\Omega_{m0}$



Left:  $L_X - L_{UV}$  relation; Right:  $R - L$  relation (Khadka, Zajaček et al., MNRAS in print)

## $R - L$ vs. $L_X - L_{UV}$ relation

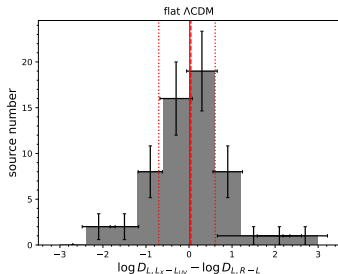
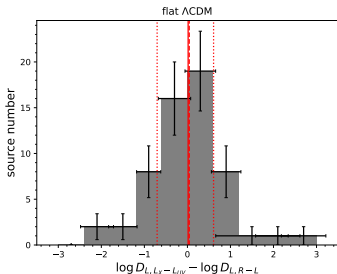
- a sample of 58 X-ray detected reverberation-mapped quasars
- systematic differences between the two relations
- $L_X - L_{UV}$  shows preference for high  $\Omega_{m0}$



Likelihood distributions for  $\Lambda$ CDM (Khadka, Zajaček et al., MNRAS in print)

## $R - L$ vs. $L_X - L_{UV}$ relation

- normally, both relations should give the same luminosity distance to the same source
- however, we obtain non-zero median luminosity distance difference  $\log D_{L,L_X-L_{UV}} - \log D_{L,R-L}$ , systematically positive



### Simple formula for UV/X-ray colour index:

$$E_{X-UV} = 2.172(1 - \gamma') < (\log D_{L,L_X-L_{UV}} - \log D_{L,R-L})_{\text{ext}} >$$

**MASARYK  
UNIVERSITY**